Chinese Chemical Letters 35 (2024) 109345

Contents lists available at ScienceDirect

Chinese Chemical Letters

journal homepage: www.elsevier.com/locate/cclet

Superatomic Ag_{58} nanoclusters incorporating a $[MS_4@Ag_{12}]^{2+}$ (M = Mo or W) kernel show aggregation-induced emission

Jun-Jie Fang, Zheng Liu, Yun-Peng Xie*, Xing Lu*

State Key Laboratory of Materials Processing and Die & Mould Technology, School of Materials Science and Engineering, Huazhong University of Science and Technology, Wuhan 430074, China

ARTICLE INFO

Article history:
Received 16 October 2023
Revised 14 November 2023
Accepted 27 November 2023
Available online 2 December 2023

Keywords:
Superatom
Silver nanocluster
Template synthesis
Photoluminescence
Aggregation-induced emission

ABSTRACT

In core-shell silver nanoclusters, the control of core structure presents a more formidable challenge compared to that of the shell structure. Here, we report the successful synthesis and characterization of four distinct silver thiolate nanoclusters $[MS_4@Ag_{12}@Ag_{46}S_{24}(dppb)_{12}]$ (M = Mo or W), each incorporating a cup-like $[MS_4@Ag_{12}]^{2+}$ kernel. These nanoclusters were meticulously prepared using $(NH_4)_2MoS_4$ or $(NH_4)_2WS_4$ as both a template and a controlled source of S^{2-} ions. Remarkably, we have observed a unique configuration within these eight-electron superatomic Ag_{58} nanoclusters, where the zero-valent Ag atoms reside exclusively within the inner $[MS_4@Ag_{12}]^{2+}$ kernel. This stands in contrast to other superatomic clusters possessing an Ag(0) core. Notably, the introduction of phenyl-containing compounds during the synthesis process induced a transformation in the space group symmetry from *C*2/*c* to $I\bar{4}$. This transformative effect was found to originate from the interplay between adjacent 1,4-bis(diphenylphosphino)butane (dppb) ligands, which facilitated enhanced emission through aggregation-induced intermolecular interactions, specifically C–H···π interactions. Collectively, our findings contribute substantively to the understanding of the intricate relationship between nanocluster structures and their corresponding properties, shedding light on the crucial roles played by templates and diphosphine ligands in this context.

Atomically precise metal nanoclusters (NCs) have garnered significant attention in both fundamental and applied sciences, owing to their exceptional physical and chemical properties. These NCs have been extensively studied in areas such as catalysis [1], optics [2] and magnetism [3]. The precise atomic arrangement within these clusters offers a unique platform for investigating the intricate relationship between structure and properties [4]. However, achieving precise control over the properties and functionalities of these NCs by manipulating atoms and molecules within their crystal structures remains a significant challenge [5]. In recent years, template-assisted synthesis of NCs has emerged as a promising approach, primarily due to its potential for achieving structural predictability [6–8]. Unlike conventional surface-protecting ligands such as thiols [9,10], phosphines [11,12], alkynyls [13,14], and calixarenes [15,16], templates enable the aggregation of multiple metal cations, leading to the formation of cluster species with captivating structures and diverse properties [17]. This avenue opens up exciting opportunities for exploring novel NC structures and uncovering their associated properties.

In previous studies, a diverse set of templates has been explored for the construction of high-nuclear silver clusters. This includes silver sulfide units [18], halogens [19,20], rare earth ions [21], acid anions [22,23], and oxometalates [24]. Among them, polyoxometalates, characterized by an abundance of terminal oxygen atoms and high charge densities, have emerged as particularly effective templates for facilitating the aggregation of additional [6,7]. In a significant contribution, Wang *et al.* demonstrated that the addition of $PhCO_2H$ triggers the transformation of $[Mo_8O_{28}@Ag_{50}]$ into $[Mo_6O_{22}@Ag_{44}]$ cluster [25]. Similarly, Shen *et al.* highlighted the role of anionic templates in tuning the photoluminescence (PL) properties of Ag_{33} clusters [24].

Conversely, there has been mounting research interest in mixed-valence Ag(0)/Ag(I) silver nanoclusters due to their intriguing structures and unique physicochemical properties. However, these clusters often suffer from poor stability attributed to the presence of partial Ag(0) characters [10,26,27]. To address this, improved synthetic approaches involving co-protection of various ligands, especially thiolates and phosphines, have proven effective in

* Corresponding authors.
E-mail addresses: xieyp@hust.edu.cn (Y.-P. Xie), lux@hust.edu.cn (X. Lu).

https://doi.org/10.1016/j.cclet.2023.109345
1001-8417/

enhancing the stability of silver clusters such as Ag_{29} [12], Ag_{40} [28], Ag_{46} [29], Ag_{50} [30], Ag_{67} [11], Ag_{78} [31].

Despite these advancements, there remains a dearth of investigations focusing on the incorporation of templates in mixed-valence Ag(0)/Ag(I) clusters. Wang *et al.* observed that the formation of octahedral Ag_6^{4+} kernel and various molybdates can be disrupted by the presence of *N*,*N*-dimethylformamide (DMF) solvent [32]. Furthermore, Duan *et al.* identified the crucial roles played by oxometalates and phosphines in the formation of twenty-electron silver nanoclusters [33]. Additionally, Liu *et al.* reported the utilization of Ag_6S unit as a template in the synthesis of Ag_{46} clusters [34]. Jin *et al.* uncovered the presence of $Ag_{14}S_{12}$ kernel in $Ag_{62}S_{12}$ clusters and $Ag_{14}S_{13}$ kernel in $Ag_{62}S_{13}$ clusters, leading to different numbers of valence electrons and subsequent variations in their PL properties [35,36]. Lastly, Wang *et al.* successfully synthesized $Ag_6Z_4@Ag_{36}$ (Z = S or Se) clusters [37] through the controlled introduction of Ph_3CSH or Ph_3PSe, which gradually release S^{2-} or Se^{2-}.

We have devised innovative strategies for the synthesis of a novel class of Ag NCs, utilizing $NaBH_4$ as the reducing agent. In our synthetic approach, $(NH_4)_2MS_4$ (M = Mo or W) serves a dual role as both a template and a slow-release reagent for S^{2-} ions, while dppb acts as protective ligands, imparting stability to the NCs. Through meticulous isolation and characterization efforts, we have successfully identified and confirmed the formulas of four distinct silver nanoclusters: $[(MoS_4)@Ag_{12}@Ag_{46}S_{24}(dppb)_{12}]$ (**1**: C2/*c* space group; **3**: $I\bar{4}$ space group), $[(WS_4)@Ag_{12}@Ag_{46}S_{24}(dppb)_{12}]$ (**2**: C2/*c* space group; **4**: $I\bar{4}$ space group). In contrast to most other superatomic nanoclusters where the zero-valent Ag atoms occupy central positions, the distinctive feature of these eight-electron superatoms lies in the MS_4^{2-} (M = Mo or W) template positioned at the center. The zero-valent Ag atoms of these Ag_{58} NCs are situated within the inner $[MoS_4@Ag_{12}]^{2+}$ kernel. Notably, intermolecular C–H···π interactions between adjacent clusters can induce a space group transformation from C2/*c* to $I\bar{4}$, further elucidating the structural intricacies. An intriguing observation is the aggregation-induced emission enhancement (AIEE) exhibited by these silver nanoclusters. By reducing the polarity of the solvent or introducing compounds containing phenyl groups, we achieve AIEE, amplifying their luminescent properties.

The novel silver NCs **1**–**4** were successfully synthesized using a convenient one-pot method, and detailed experimental procedures can be found in Supporting information. Single-crystal X-ray diffraction (SCXRD) analysis revealed that the main structural motifs of **1** and **2** were analogous to those of NCs **3** and **4**, albeit with different space group symmetry; specifically, **1** and **2** exhibited the C2/c space group, while **3** and **4** adopted the $I\bar{4}$ space group. Comprehensive crystallographic data and structure refinement details for **1**–**4** are provided in Tables S1 and S2 (Supporting information).

Crystals of **1**–**4** exhibit high solubility in MeOH and CH_2Cl_2, enabling a detailed investigation of their solution behaviors through electrospray ionization mass spectrometry (ESI-MS). In the positive ion mode ESI-MS analysis of **1**, a distinct peak at $m/z = 4128.50$ corresponding to the three-charge state $[\mathbf{1b}]^{3+}$ was observed. This peak can be confidently attributed to the species $[(MoS_4)@Ag_{12}@Ag_{46}S_{24}(dppb)_{11} + 3Ag^+ + CH_2Cl_2 + CH_3OH]^{3+}$ (sim. $m/z = 4128.39$). Furthermore, the peak at $m/z = 3123.53$, corresponding to the four-charge state $[\mathbf{1a}]^{4+}$, was identified as $[(MoS_4)@Ag_{12}@Ag_{46}S_{24}(dppb)_{11} + 4Ag^+ + CH_2Cl_2 + CH_3OH]^{4+}$ (sim. $m/z = 3123.52$). Similarly, in the positive ion mode ESI-MS analysis of **2**, prominent peaks at $m/z = 3061.67$ ($[\mathbf{2a}]^{4+}$), 4118.54 ($[\mathbf{2b}]^{3+}$), and 4129.19 ($[\mathbf{2c}]^{3+}$) were observed. These peaks correspond to the species $[(WS_4)@Ag_{12}@Ag_{46}S_{24}(dppb)_{11} + 2Ag^+ + 2H^+]^{4+}$ (sim. $m/z = 3062.84$), $[(WS_4)@Ag_{12}@Ag_{46}S_{24}(dppb)_{11} + 3Ag^+]^{3+}$ (sim. $m/z = 4118.41$), and $[(WS_4)@Ag_{12}@Ag_{46}S_{24}(dppb)_{11} + 3Ag^+ + CH_3OH]^{3+}$ (sim. $m/z = 4129.09$), respectively (Fig. 1 and Fig. S1 in Supporting information). Importantly, these species arise from the incorporation of three Ag^+ ions and solvent molecules subsequent to the removal of a single dppb ligand from the pristine cluster. These assignments are consistent with the data obtained from single-crystal X-ray diffraction analysis. Other characterizations including elemental analysis (EA), powder XRD, thermogravimetric (TG) analysis, Fourier-transform infrared (FT-IR) spectra, and X-ray photoelectron spectroscopy (XPS) were analyzed in Figs. S2–S5 (Supporting information).

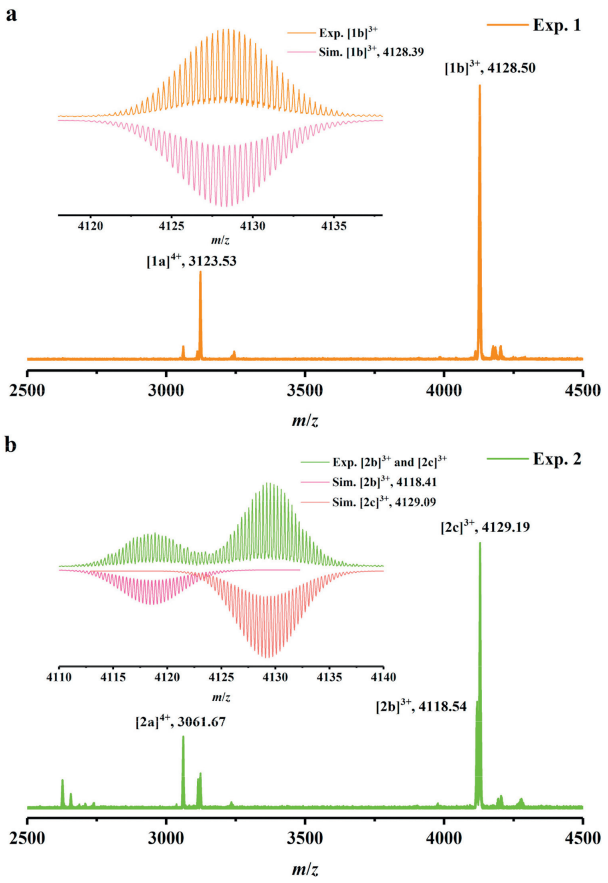

Fig. 1. Experimental isotope distributions of selected peaks for (a) **1** and (b) **2** (positive ion mode, dissolved in CH_3OH and CH_3CN).

Single-crystal X-ray analysis revealed that NCs **1**–**4** are neutral silver nanoclusters consisting of 58 Ag atoms. They exhibit a tetrahedral structural motif, comprising a central MS_4^{2-} (M = Mo or W) template, twenty-four bridging S^{2-} ions, and twelve dppb ligands. The MS_4 tetrahedron containing the Mo or W atom exhibits disorder, indicating significant vibrational motion within the tetrahedral framework at low temperatures. Although the structures of all four NCs are similar, a detailed description will be provided for **1** for clarity. In order to enhance visual understanding, Fig. 2 depicts a schematic representation of the crystal structure, with the average positions of the Mo atoms.

As depicted in Fig. 2, NC **1** features a multi-shell core architecture encapsulating a $[MoS_4@Ag_{12}@Ag_{46}S_{24}(dppb)_{12}]$ motif. Notably, the encapsulated MoS_4^{2-} anion template is housed within an irregular Ag_{12} shell, distinct from the conventional M_{12} (M = Au or Ag) icosahedral structures reported in previous literature [27,38]. This observation highlights the substantial structural influence exerted by the introduction of templates on the core architecture. Each of the four S atoms from the template is coordinated to three Ag atoms, leading to the formation of the $MoS_4@Ag_{12}$ kernel, characterized by argentophilic Ag–Ag bond distances ranging from 2.870 Å to 3.217 Å. The observed Ag–S_{Mo} (S_{Mo} = sulfur atom of the

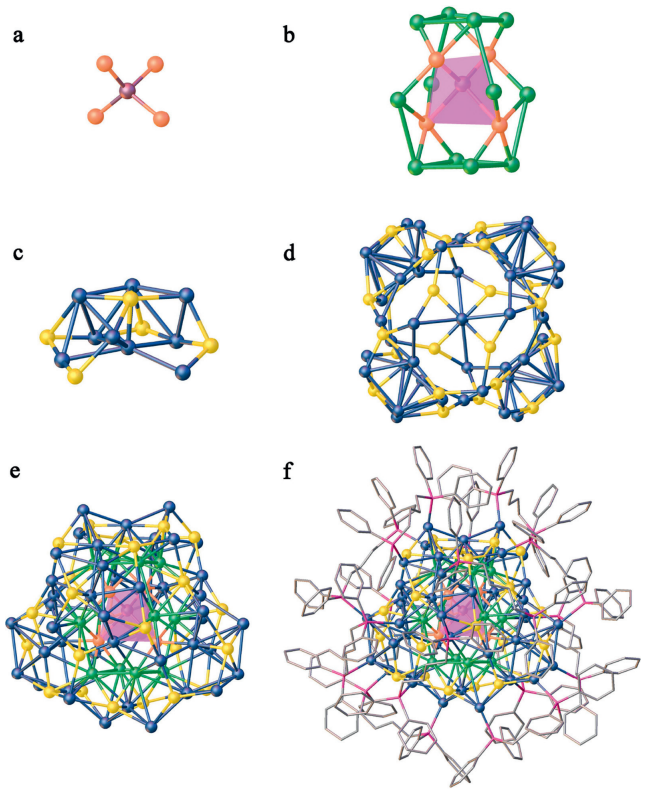

Fig. 2. (a) MoS_4^{2-} anion template. (b) Cup-like $[MoS_4@Ag_{12}]^{2+}$ kernel (MoS_4 tetrahedra are highlighted in pink). (c) "Wind blade"-like Ag_9S_5 unit of $Ag_{46}S_{24}$ shell. (d) "Windmill" shaped $Ag_{46}S_{24}$ shell. (e) Multishelled core architecture of $[MoS_4@Ag_{12}@Ag_{46}S_{24}]$ skeleton. (f) Overview of the total structure of $[MoS_4@Ag_{12}@Ag_{46}S_{24}(dppb)_{12}]$. Color codes: Mo, brown; Ag, green and dark blue; S, orange and yellow; P, purple; C, gray; Hydrogen atoms are omitted for clarity.

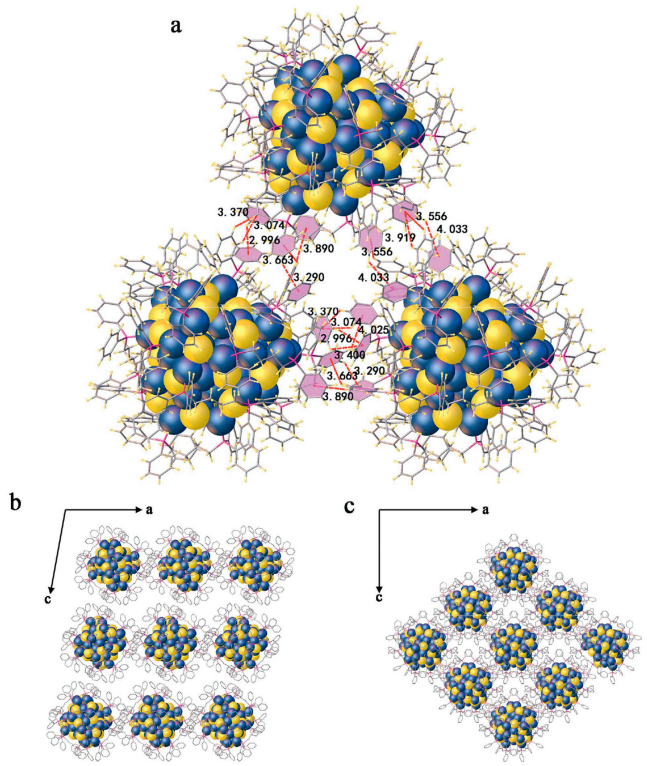

Fig. 3. (a) The intermolecular C−H···π interactions (Å) between dppb ligands of adjacent clusters in **1** (phenyl groups with interactions are highlighted in pink). (b, c) Cluster packing patterns along the *b* axis of **1** (*C*2/*c*) and **3** ($I\bar{4}$). Color codes: Ag, dark blue; S, yellow; P, purple; C, gray; Hydrogen atoms are omitted for clarity.

MoS_4^{2-} anion template) bond lengths and average Mo−S bond lengths are 2.552−2.920 and 2.530 Å, respectively. As depicted in Figs. 2d and e, the $MoS_4@Ag_{12}$ kernel is further surrounded by an $Ag_{46}S_{24}$ shell resembling a "windmill" shape. The Ag−Ag and Ag−S bond lengths between the $MoS_4@Ag_{12}$ kernel and $Ag_{46}S_{24}$ shell span from 2.8893 Å to 3.350 Å and from 2.427 Å to 2.870 Å, respectively. The "windmill"-shaped $Ag_{46}S_{24}$ shell consists of four "wind blade"-like Ag_9S_5 units, which are interconnected through two distinct bridging coordination modes (Fig. S6 in Supporting information). Each of the six S^{2-} ions adopts a μ_4 ligation mode, bridging four surrounding Ag atoms, while the remaining eighteen S^{2-} ions coordinate to five Ag atoms through a μ_5 ligation mode, with Ag−S distances ranging from 2.308 Å to 2.943 Å (Fig. S7 in Supporting information). Notably, argentophilic Ag−Ag interactions are observed, with Ag−Ag distances ranging from 2.992 Å to 3.266 Å.

In the context of the multishelled core architecture $[MoS_4@Ag_{12}@Ag_{46}S_{24}]$, it is observed that each of the twelve dppb ligands coordinates to an Ag atom on the $Ag_{46}S_{24}$ shell through Ag−P bonds, with bond lengths ranging from 2.393 Å to 2.457 Å. The bidentate phosphine ligands, characterized by differing lengths, exhibit distinct coordination modes on the surface of Ag clusters [30,39]. As illustrated in Fig. S8 (Supporting information), four distinct staple motifs involving dppb ligands, Ag atoms, and S atoms were identified in **1**, namely Ph_2P−Ag−Ag−Ag−PPh_2, Ph_2P−Ag−S−Ag−PPh_2, Ph_2P−Ag−Ag−S−Ag−PPh_2, and Ph_2P−Ag−S−Ag−S−Ag−PPh_2.

These specific coordination modes of dppb ligands contribute to the protection of the cluster surface, reduction of surface energy, and enhancement of stability. According to the "superatom" theory [40], the total electron count for the $[(MS_4)@Ag_{58}S_{24}(dppb)_{12}]$ (M = Mo or W) cluster is calculated to be 8, which arises from $[(58 \times 1) - (24 \times 2) - 2] = 8$. Notably, 8 corresponds to a magic number based on the electronic cluster shell model [41], following an Aufbau rule of $1S^2|1P^6|$. This shell closure typically exhibits a significant energy gap between the highest occupied molecular orbitals (HOMO) and the lowest unoccupied molecular orbitals (LUMO), thereby contributing to the enhanced stability of ligand-protected metal clusters [27,33,38].

The surfaces of NCs **1**−**4** are abundantly decorated with phenyl groups, giving rise to a diverse array of C−H···π intermolecular interactions between adjacent nanoclusters. In **1**, these interactions are observed within a range of 2.996−4.033 Å, while in **2**, they span from 2.929−3.975 Å. Similarly, in **3**, the range is 2.947−4.086 Å, and in **4**, it is 2.912−4.039 Å (Fig. 3a and Fig. S9 in Supporting information).

In an effort to synthesize **3** and **4**, which possess the same cluster structure as **1** and **2** but belong to different space groups, $PhCO_2H$, $PhCO_2K$, $PhPO_3H_2$, or $PhPO_3Na_2$ were introduced to the synthesis system of **1** and **2**. The successful synthesis of **3** and **4** with higher yields suggests that the addition of these compounds containing phenyl groups facilitates the aggregation and crystallization of the nanoclusters during the assembly process. This phenomenon can be attributed to the favorable $\pi\cdots\pi$ or C−H···π interactions between these compounds and the surface ligands of the nanoclusters, effectively restricting the mobility of the nanoclusters and enhancing their crystallization propensity. Furthermore, these interactions induce a transition in the cluster's space group from *C*2/*c* to $I\bar{4}$ (Figs. 3b and c, and Fig. S10 in Supporting information).

Notably, despite the similarities in structures among **1**−**4**, there exist variations in average bond lengths attributable to distinct core structures and space groups. In **2**, for instance, the W−S average bond length within the WS_4 tetrahedra is measured at 2.593 Å, slightly longer than the Mo−S bond length (2.530 Å) observed in

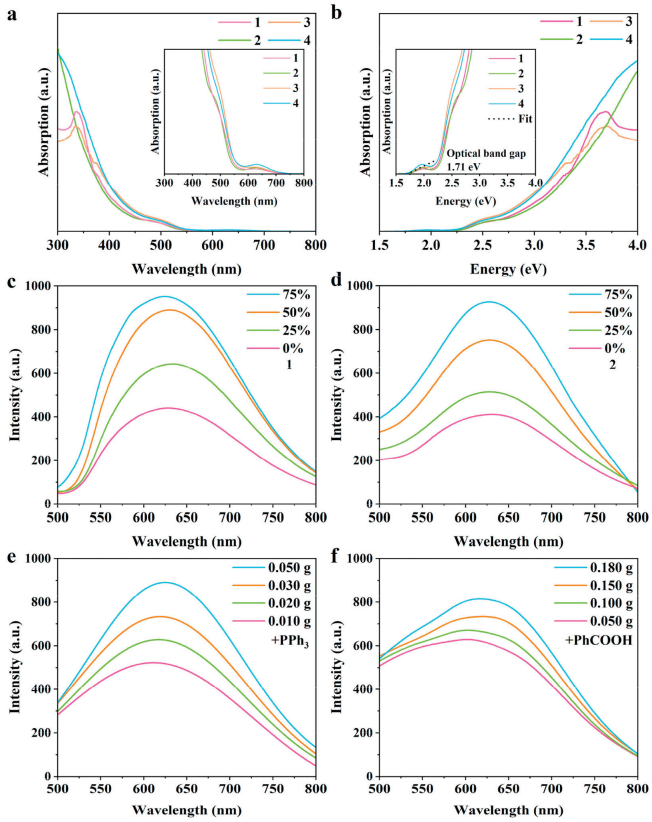

Fig. 4. (a, b) UV-vis spectra of **1**–**4**. Emission spectra of (c) **1** and (d) **2** (dissolved in THF and MeOH, and the volume fraction of THF is 0%, 25%, 50%, and 75%, respectively; all excited by 480 nm light). (e, f) Emission spectra of **2** (added different quality of PPh_3) and **2** (added different quality of $PhCO_2H$).

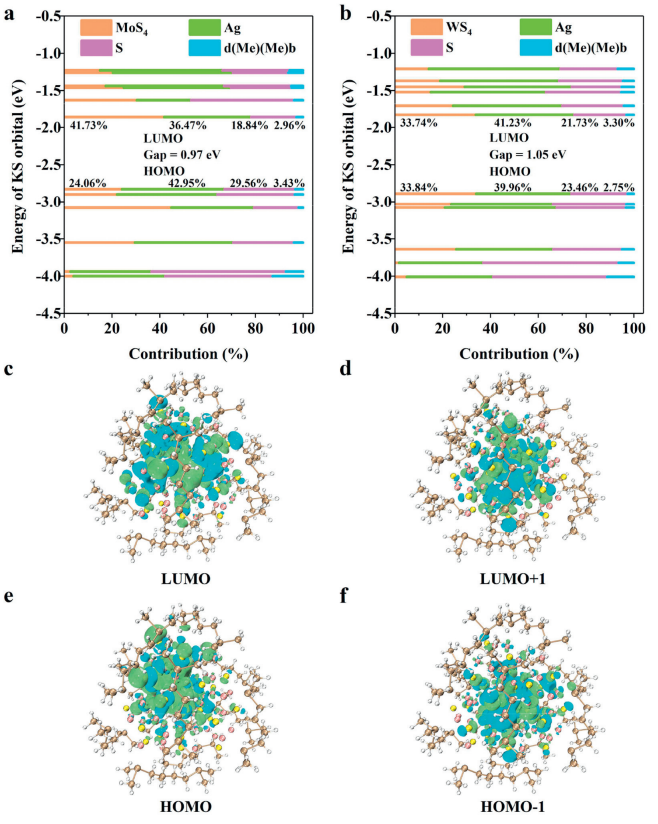

Fig. 5. (a, b) Composition analysis of frontier Kohn–Sham orbitals of **1** and **2**. Electronic density diagrams of the (c) LUMO, (d) LUMO+1, (e) HOMO, (f) HOMO-1 of **1** (isovalue = 0.01 a.u.). The phenyl groups present in the dppb ligands were selectively replaced with methyl groups, abbreviated as d(Me)(Me)b.

1. As for **3**, the average bond lengths of Ag–Ag and Ag–S are recorded as 2.913 Å and 2.448 Å, respectively. These values indicate a reduction compared to the corresponding bond lengths in **1**, namely Ag–Ag (3.068 Å) and Ag–S (2.553 Å). Likewise, **4** exhibits shorter average bond lengths of Ag–Ag (3.044 Å) and Ag–S (2.469 Å) compared to **2**, where the corresponding lengths are Ag–Ag (3.057 Å) and Ag–S (2.524 Å). These observations suggest that the transition from the *C*2/*c* to $I\bar{4}$ space group leads to a contraction in average bond lengths. It is worth noting that differences in core structure and space group do not induce alterations in the coordination patterns of S^{2-} ions and dppb ligands on the surface.

The UV-vis absorption spectra of **1**–**4** exhibit two distinct peaks in the ranges of 475–520 and 600–650 nm (Figs. 4a and b). The presence of these similar absorption characteristic peaks indicates their comparable electronic structures [23]. Luminescence, a critical property of silver clusters, holds significant potential for applications in molecular sensing, detection, and imaging [42–44]. Therefore, we conducted an extensive investigation into the emission properties of these Ag_{58} NCs in solution. When excited with 480 nm light at room temperature, **1** dissolved in methanol demonstrates a broad emission band centered at 625 nm, while **2** exhibits an emission peak at 630 nm (Figs. 4c and d, Figs. S11 and S12 in Supporting information). Although **1** and **2** display similar PL emission spectra, the emission peak of **2** is red-shifted by 5 nm compared to that of **1**. This phenomenon can be attributed to the differential templates encapsulated within the identical silver-thiolate framework [45,46].

To gain further insight into the PL mechanism, we performed density functional theory (DFT) calculations employing the ORCA 5.0.3 program [47] and Multiwfn 3.8 program [48]. In these calculations, the phenyl groups present in the dppb ligands were selectively replaced with methyl groups to reduce computational costs. Fig. 5 and Fig. S13 (Supporting information) provide the results obtained, revealing HOMO–LUMO band gaps of 0.97 eV for **1** and 1.05 eV for **2**, consistent with the value of 1.2 eV reported for the eight-electron $Au_{25}(SMe)_{18}$ cluster [49]. Comparative analysis further indicates that **1** and **2** exhibit similar arrangements of electron clouds in their Kohn-Sham orbitals, as well as contributions from different components to the LUMO and HOMO. The PL mechanism is attributed to the MS_4 (M = Mo or W) → Ag charge transfer process, which is modified by the presence of outer S^{2-} ions and dppb ligands within the crystal structure.

The surfaces of Ag_{58} nanoclusters are adorned with numerous phenyl groups, establishing a foundation for exploring their AIE activities. To examine these behaviors, the nanoclusters were investigated in a MeOH/THF (tetrahydrofuran) solvent system. In each experiment, 5 mg of freshly prepared crystals were dissolved in 10 mL of solvent. By modulating the polarity of the mixed solvent system, the aggregation degree could be controlled. Specifically, increasing the volume fraction of THF ($f = vol_{THF}/vol_{MeOH+THF}$) led to decreased polarity and a higher degree of aggregation. The observed results, depicted in Figs. 4c and d, were achieved through deliberate manipulation of these variables. With an increase in *f*, the PL intensities of **1** and **2** exhibited corresponding increments, accompanied by blue shifts of the emission peaks by 3–5 nm, suggesting a progressive enlargement of the assembly size under the influence of the solvent [50].

Furthermore, the addition of PPh_3 or $PhCO_2H$ to MeOH solvent of **2** yielded similar results of AIEE (Figs. 4e and f). For each experiment, 5 mg of freshly prepared crystals were dissolved in 10 mL of MeOH, followed by thorough stirring upon addition of PPh_3

or $PhCO_2H$. The phenyl groups present in PPh_3 and $PhCO_2H$ facilitated abundant $\pi\cdots\pi$ and C−H···π intermolecular interactions with the numerous dppb ligands on the cluster's surface. Consequently, these interactions induced aggregation of the Ag_{58} clusters in the solvent, leading to enhanced PL intensity. It can be inferred that the C−H···π intermolecular interactions between adjacent molecules effectively curtail intramolecular rotations and vibrations. This constraint significantly enhances the radiative transition of the aggregated state, ultimately culminating in the observed AIE behavior. Overall, this AIE property emerges from the restricted intramolecular rotation (RIR) mechanism [51].

In summary, we have successfully synthesized and characterized four novel silver thiolate nanoclusters, employing template-assisted strategies. These strategies involve the utilization of $(NH_4)_2MoS_4$ or $(NH_4)_2WS_4$ as both templates and slow chalcogen-release reagents. The resulting nanoclusters exhibit an eight-electron superatom nature and possess a multishelled core architecture denoted as $[MS_4@Ag_{12}@Ag_{46}S_{24}(dppb)_{12}]$ (M = Mo or W). Our study demonstrates the achievement of the AIEE through intermolecular C−H···π interactions present on the surfaces of nanoclusters **1**–**4**. This effect can be realized by reducing the polarity of the solvent or introducing phenyl-containing compounds. Importantly, we highlight the significant role played by templates and dppb ligands in directing the construction of silver thiolate clusters with distinct optical properties. Furthermore, this work paves the way for exploring the intricate relationship between cluster structures and their associated properties, thereby opening new avenues for future investigations in this field.

Declaration of competing interest

The authors declare that they have no known competing financial interests or personal relationships that could have appeared to influence the work reported in this paper.

Acknowledgments

We gratefully acknowledge financial support from the National Natural Science Foundation of China (Nos. 21771071, 22171094, 21925104, and 92261204) and the Hubei Provincial Natural Science Foundation of China (No. 2021CFA020). We thank the staff in the Analytical and Testing Center at the Huazhong University of Science and Technology for all related measurements. We thank the staff at the BL17B beamline of the National Center for Protein Sciences Shanghai (NCPSS) at Shanghai Synchrotron Radiation Facility for the assistance with data collection.

Supplementary materials

The X-ray crystallographic data for **1**–**4** have been deposited at the Cambridge Crystallographic Data Centre (CCDC), under deposition number 2193459, 2193586, 2193591, and 2193473.

Supplementary material associated with this article can be found, in the online version, at doi:10.1016/j.cclet.2023.109345.

References

[1] S.S. Wang, G.Y. Yang, Chem. Rev. 115 (2015) 4893–4962.
[2] P. Yuan, R. Zhang, E. Selenius, et al., Nat. Commun. 11 (2020) 2229.
[3] S. Bao, L. Zheng, Coord. Chem. Rev. 319 (2016) 63–85.
[4] D.A. Tomalia, S.N. Khanna, Chem. Rev. 116 (2016) 2705–2774.
[5] H. Liu, C. Song, R. Huang, et al., Angew. Chem. Int. Ed. 55 (2016) 3699–3703.
[6] Y. Xie, T.C.W. Mak, J. Am. Chem. Soc. 133 (2011) 3760–3763.
[7] Y. Xie, T.C.W. Mak, Angew. Chem. Int. Ed. 51 (2012) 8783–8786.
[8] Z. Wang, H. Su, Y. Gong, et al., Nat. Commun. 11 (2020) 308.
[9] C.P. Joshi, M.S. Bootharaju, M.J. Alhilaly, et al., J. Am. Chem. Soc. 137 (2015) 11578–11581.
[10] R.S. Dhayal, J. Liao, Y. Liu, et al., Angew. Chem. Int. Ed. 54 (2015) 3702–3706.
[11] M.J. Alhilaly, M.S. Bootharaju, C.P. Joshi, et al., J. Am. Chem. Soc. 138 (2016) 14727–14732.
[12] L.G. AbdulHalim, M.S. Bootharaju, Q. Tang, et al., J. Am. Chem. Soc. 137 (2015) 11970–11975.
[13] G. Duan, L. Tian, J. Wen, et al., Nanoscale 10 (2018) 18915–18919.
[14] M. Qu, H. Li, L. Xie, et al., J. Am. Chem. Soc. 139 (2017) 12346–12349.
[15] D. Geng, X. Han, Y. Bi, et al., Chem. Sci. 9 (2018) 8535–8541.
[16] Y. Bi, S. Du, W. Liao, Coord. Chem. Rev. 276 (2014) 61–72.
[17] J. Liu, H. Su, Z. Wang, et al., Chem. Commun. 54 (2018) 4461–4464.
[18] Y. Xie, J. Jin, X. Lu, et al., Angew. Chem. Int. Ed. 54 (2015) 15176–15180.
[19] Z. Qin, D. Zhao, L. Zhao, et al., Nanoscale Adv. 1 (2019) 2529–2536.
[20] L. Ren, P. Yuan, H. Su, et al., J. Am. Chem. Soc. 139 (2017) 13288–13291.
[21] G. Duan, Y. Xie, J. Jin, et al., Chem. Eur. J. 24 (2018) 6762–6768.
[22] M. Zhao, S. Huang, Q. Fu, et al., Angew. Chem. Int. Ed. 59 (2020) 20031–20036.
[23] J.S. Yang, Z. Han, X.Y. Dong, et al., Angew. Chem. Int. Ed. 59 (2020) 11898–11902.
[24] Y.L. Shen, J.L. Jin, G.X. Duan, et al., Chem. Eur. J. 27 (2021) 1122–1126.
[25] Z. Wang, H. Su, C. Tung, et al., Nat. Commun. 9 (2018) 4407.
[26] H. Yang, Y. Wang, X. Chen, et al., Nat. Commun. 7 (2016) 12809.
[27] A. Desireddy, B.E. Conn, J. Guo, et al., Nature 501 (2013) 399–402.
[28] X. Yuan, C. Sun, X. Li, et al., J. Am. Chem. Soc. 141 (2019) 11905–11911.
[29] M. Bodiuzzaman, A. Ghosh, K.S. Sugi, et al., Angew. Chem. Int. Ed. 58 (2019) 189–194.
[30] W. Du, S. Jin, L. Xiong, et al., J. Am. Chem. Soc. 139 (2017) 1618–1624.
[31] H. Yang, J. Yan, Y. Wang, et al., J. Am. Chem. Soc. 139 (2017) 16113–16116.
[32] Z. Wang, H. Su, M. Kurmoo, et al., Nat. Commun. 9 (2018) 2094.
[33] G. Duan, J. Han, B. Yang, et al., Nanoscale 12 (2020) 1617–1622.
[34] X. Liu, J. Chen, J. Yuan, et al., Angew. Chem. Int. Ed. 57 (2018) 11273–11277.
[35] S. Jin, S. Wang, L. Xiong, et al., Chem. Mater. 28 (2016) 7905–7911.
[36] S. Jin, S. Wang, Y. Song, et al., J. Am. Chem. Soc. 136 (2014) 15559–15565.
[37] Z. Wang, J. Liu, H. Su, et al., J. Am. Chem. Soc 141 (2019) 17884–17890.
[38] H. Yang, Y. Wang, H. Huang, et al., Nat. Commun. 4 (2013) 2422.
[39] F. Tian, R. Chen, J. Am. Chem. Soc. 141 (2019) 7107–7114.
[40] M. Walter, J. Akola, O. Lopez-Acevedo, et al., Proc. Natl. Acad. Sci. U. S. A. 105 (2008) 9157–9162.
[41] B. Yoon, P. Koskinen, B. Huber, et al., ChemPhysChem 8 (2007) 157–161.
[42] T. Chen, S. Yang, J. Chai, et al., Sci. Adv. 3 (2017) e1700956.
[43] N. Goswami, Q. Yao, Z. Luo, et al., J. Phys. Chem. Lett. 7 (2016) 962–975.
[44] Y. Xie, Y. Shen, G. Duan, et al., Mater. Chem. Front. 4 (2020) 2015–2222.
[45] X. Kang, M. Zhu, Chem. Soc. Rev. 48 (2019) 2422–2457.
[46] Z. Chen, N. Zhao, Y. Fan, et al., Coord. Chem. Rev. 253 (2009) 1–20.
[47] F. Neese, F. Wennmohs, U. Becker, et al., J. Chem. Phys. 152 (2020) 224108.
[48] T. Lu, F. Chen, J. Comput. Chem. 33 (2012) 580–592.
[49] J. Akola, M. Walter, R.L. Whetten, et al., J. Am. Chem. Soc. 130 (2008) 3756–3757.
[50] Y. Zhang, D. Li, Y. Li, et al., Chem. Sci. 5 (2014) 2710.
[51] Q. Zhang, D. Li, X. Li, et al., J. Am. Chem. Soc. 138 (2016) 13541–13550.